Cellular and Molecular Life Sciences (2025) 82:303
https://doi.org/10.1007/s00018-025-05790-x

ORIGINAL ARTICLE

PGC1α regulates the mitochondrial metabolism response to cyclic stretch, which inhibits neointimal hyperplasia

Minwen Zou[1] · Kaichuang Ye[2] · Jing Yan[1] · Shoumin Zhang[1] · Han Bao[1] · Zhiyin Li[1] · Yuting Tao[1] · Xing Zhang[2] · Wenhao Tian[1] · Yingxin Qi[1] · Yunlong Huo[1] · Yue Han[1]

Received: 26 September 2024 / Revised: 19 May 2025 / Accepted: 9 June 2025

Abstract

Neointimal hyperplasia occurs in the context of vascular injury, such as stent intervention or balloon angioplasty. However, the role of mechanical forces in this process remains to be studied. In this study, a rat carotid artery intimal injury model was established. RNA-sequencing and transmission electron microscopy revealed that intimal injury disrupted the balance of vascular energy metabolism and impaired the mitochondrial ultrastructure in vivo. The human carotid plaque and femoral artery plaque samples also exhibited alterations in mitochondrial morphology. Vascular smooth muscle cells (VSMCs) are the main components of neointimal hyperplasia and are subjected to cyclic stretch resulting from pulsatile pressure. In this study, we found that the application of cyclic stretch in vitro increased VSMC mitochondrial mass and function. In addition, peroxisome proliferator-activated receptor gamma coactivator-1α (PGC1α) played an important role in regulating VSMC mitochondrial function in response to physiological stretch via the phosphorylation of Smad3. Increasing the activation of PGC1α by ZLN005 treatment effectively inhibited VSMC hyperproliferation after intimal injury in vivo. These results suggested that the regulation of PGC1α by p-Smad3 in response to physiological cyclic stretch may effectively alleviate neointimal hyperplasia by promoting mitochondrial function. PGC1α may be a potential therapeutic target for the prevention and treatment of neointimal hyperplasia.

Keywords Vascular injury · Vascular smooth muscle cells · Cyclic stretch · Mitochondrial energy metabolism · PGC1α · Mechanotransduction

Abbreviations

AMI	acute myocardial infarction
ATP	adenosine triphosphate
BP	biological processes
CC	cellular components
CS	cyclic stretch
DAPI	diamidine-2-phenylindole dihydrochloride
DRP1	dynamin-related protein 1
EC	endothelial cell
ECL	enhanced chemiluminescence
ETC	electron transport chain
FDR	false discovery rate
GO	gene ontology
HA-VSMC	human aortic vascular smooth muscle cells
HE staining	hematoxylin–eosin staining
IPA	ingenuity pathway analysis
KEGG	kyoto encyclopedia of genes and genomes
Mdivi-1	mitochondrial mitogenic inhibitor 1
MFN2	mitochondrial fusion protein 2
MIRI	myocardial ischemia/reperfusion injury
OXPHOS	oxidative phosphorylation
CABG	coronary artery bypass grafting
PCI	percutaneous coronary intervention
PGC1α	peroxisome proliferator-activated receptor

Minwen Zou, Kaichuang Ye, Jing Yan and Shoumin Zhang contributed equally to this work.

✉ Yunlong Huo
huoyunlong@sjtu.edu.cn

✉ Yue Han
hanyue625@sjtu.edu.cn

[1] Institute of Mechanobiology and Medical Engineering, School of Life Sciences & Biotechnology, Shanghai Jiao Tong University, Shanghai, China

[2] Department of Vascular Surgery, Shanghai Ninth People's Hospital, Shanghai Jiao Tong University School of Medicine, Shanghai, China

Published online: 08 August 2025

	gamma coactivator-1α
PLS-DA	partial least squares-discriminate analysis
PPARγ	peroxisome proliferator-activated receptor gamma
qRT-PCR	quantitative real-time PCR
ROS	reactive oxygen species
SD rats	Sprague-Dawley rats
siRNA	small interfering RNA
SMA	smooth muscle-specific α-actin
TEM	transmission electron microscopy
VSMC	vascular smooth muscle cell

Introduction

Common clinical treatments for cardiovascular diseases include drug therapy, coronary artery bypass grafting (CABG), and percutaneous coronary intervention (PCI) [1]. Although surgery can effectively improve the survival rate of patients, mechanical stimulation often leads to intimal injury, which manifests mainly as excessive neointimal hyperplasia, ultimately resulting in vascular stenosis and atherosclerosis [2]. Vascular smooth muscle cells (VSMCs) are exposed to the cyclic stretch (CS) generated from cardiac pulsatility. Mechanical forces play important roles in VSMC behavior in the pathological process of neointimal hyperplasia. However, the molecular mechanisms by which CS regulates VSMC function and its ability to inhibit neointimal hyperplasia remain largely unknown.

Mitochondria are known as energy factories for the production of adenosine triphosphate (ATP) through oxidative phosphorylation (OXPHOS). Healthy mitochondria under physiological conditions are crucial for maintaining the balance between catabolism and anabolism, which maintains cellular homeostasis. Relieving mitochondrial dysfunction and restoring normal functional activity are feasible goals for cardiovascular disease treatment [3].

PGC1α is a transcriptional coactivator that regulates glucose, lipid and energy metabolism and has been found to be reduced in a variety of metabolic diseases [4]. PGC1α expression and activity are tightly controlled by multiple signaling pathways. Environmental cues, such as cold exposure, physical exercise, and other stresses, activate these signaling pathways. Although PGC1α is considered a potential therapeutic target for type II diabetes, obesity, cardiomyopathy and other metabolic diseases [5], the effects of biomechanical forces on the function of PGC1α are incompletely understood.

The overexpression of PGC1α has been shown to increase mitochondrial biosynthesis, mitochondrial respiration and ATP synthesis in skeletal muscle and cardiomyocytes [6, 7]. PGC1α also participates in the process of mitochondrial fusion and fission as a transcriptional coactivator of mitochondrial fusion protein 2 (MFN2) to regulate mitochondrial dynamics in atherosclerosis and ischemic stroke [8]. In myocardial ischemia/reperfusion injury (MIRI) and acute myocardial infarction (AMI), AMPK and SIRT1 activate PGC1α, which attenuates diseases by regulating mitochondrial oxidative stress [9, 10]. Moreover, whether PGC1α participates in regulating VSMC mitochondrial function after intimal injury occurs and what the role of mechanical stretching in this process is remain underexplored.

Hence, in the present study, we established a carotid artery injury model in Sprague–Dawley (SD) rats in vivo and applied the FX-5000T Strain Unit in vitro to investigate the role of PGC1α in mitochondrial function in VSMCs under mechanical stretch and in the process of neointimal hyperplasia. Our results suggested that PGC1α inhibited the overproliferation of VSMCs after intimal injury by regulating mitochondrial function. The aim of this study was to examine the effects of mechanical stretch on PGC1α and VSMC mitochondrial function after intimal injury and to elucidate the possible signaling pathways that participate in this process.

Materials and methods

Patients and specimens

Carotid plaque and femoral artery plaque samples were obtained from patients who underwent carotid endarterectomy and femoral artery endarterectomy at Shanghai Ninth People's Hospital (Shanghai, China). The surgery was performed according to standard procedures. The study was approved by the Ethics Committee of Shanghai Ninth People's Hospital, Shanghai Jiao Tong University, School of Medicine (approval IDs: SH9H-2019-T173-2). Studies involving patients were conducted in accordance with the ethical guidelines of the Declaration of Helsinki. Each patient provided written informed consent before enrollment in the study.

Rat carotid artery intimal injury model

The feeding and handling of the animals used in the experiment were in line with the recommendations of the 8th edition of the National Institutes of Health's Guidelines for the Care and Use of Laboratory Animals (NIH, revised 2011), were in accordance with the Animal Management Rules of China (Documentation 55, 2001, Ministry of Health, China), and were approved by the Animal Research Committee of Shanghai Jiao Tong University.

Male SD rats with an average weight of 400 g were anesthetized with isoflurane. The limbs of anesthetized rats were fixed with adhesive tape, and the left common carotid artery was exposed under a microscope. The carotid artery was subsequently exposed. A balloon (2 F, 0.67 mm, Edwards Lifesciences, Irvine, CA, USA) was used to establish vascular intimal injury. Briefly, a small incision was cut from the external carotid artery, a balloon was inserted into it, and the process of inflation and contraction was repeated three times, resulting in damage to the intima of the vessel. The common carotid arteries of the injured and contralateral sides were collected 4 weeks after surgery.

Isolation, cultivation and characterization of VSMCs

Male SD rats with an average weight of 180 g were euthanized by intraperitoneal injection of pentobarbital sodium (75 mg/kg). The thoracic aorta was isolated surgically and quickly placed in sterile DMEM (Gibco, Thermo Fisher Scientific, USA) supplemented with antibiotics (100 U/mL penicillin and 100 μg/mL streptomycin). The vessels were cut lengthways, and the intima was spread downward in DMEM culture medium containing 0.2% type I collagenase, placed in a 37 °C incubator for digestion for 5 min, then removed and changed to DMEM culture medium containing 0.3% type II collagenase for 90 min [11]. DMEM containing 10% calf serum (Gibco) supplemented with antibiotics was used to terminate digestion. The adventitia tissue was removed, and the vessel was placed in a new Petri dish with 1 mL of complete culture medium and cut into 1 mm^2 explants. The culture medium was changed every other day, and the cells were passaged after 7–8 days. Primary rat aortic VSMCs were characterized by immunofluorescence staining for the VSMC marker smooth muscle-specific α-actin (SMA) (Proteintech, China), and passages 4 to 7 of the VSMCs and cell populations with greater than 95% purity were used in the present study.

Cyclic stretch application

The FX-5000T Strain Unit (Flexcell International, USA) was used to load cyclic stretch on the VSMCs. VSMCs were grown on Flexcell silicone-bottom plates (Flexcell International, USA) at a density of 2×10^5 cells/well. The cells that reached 80% confluence were starved in serum-free DMEM for 24 h and then subjected to cyclic stretch with an elongation magnitude of 10% at a consistent frequency of 1.25 Hz for 24 h. The VSMCs without cyclic stretch loading were used as the static control group.

Western blot analysis

For the cell samples, the cell culture medium in the six-well plate was removed, and the cells were collected after washing with cold PBS and lysed with RIPA lysis buffer to obtain the protein samples (Beyotime Biotechnology, China). For tissue samples, carotid arteries were cut into tissue blocks approximately 1 mm^2 in size with spring scissors, and RIPA lysis buffer was added to the tissue, after which the lysate was collected. The samples were subsequently treated with boiling water for 7 min, and the sample volume ranged from 7 to 12 μL per well. The voltage was adjusted to 80 V for electrophoresis. After protein electrophoresis, the protein sample was transferred to a PVDF membrane at 300 mA for 2 h. After the membrane transfer was complete, the PVDF membrane was removed, placed in 5% nonfat milk and blocked in a room temperature shaker for 1 h. After blocking, primary antibodies against PGC1α (1:1000, Proteintech, China), β-actin (1:1000, Proteintech, China), Smad3 (1:1000, Cell Signaling Technology, USA), p-Smad3 (1:1000, Cell Signaling Technology, USA) and target molecules were used for incubation, and the membranes were placed in a 4 °C refrigerator overnight. On the second day, the membranes were rinsed 3 times with TBST for 10 min each and then incubated with relevant HRP-conjugated secondary antibodies (Jackson ImmunoResearch, USA) of the corresponding species at room temperature for 2 h. After washing, chemiluminescence detection was performed with an enhanced chemiluminescence (ECL) kit (Beyotime Biotechnology, China) and quantified by Image Studio.

Quantitative real-time PCR

For the cell samples, the cell culture medium in the six-well plate was removed, and protein samples were collected after washing with PBS and lysis with TRIzol (Thermo Fisher Scientific, USA). For tissue samples, carotid arteries were cut into tissue blocks approximately 1 mm^2 in size with scissors, and TRIzol was added to lyse the tissue. After the RNA was isolated, cDNA was obtained with a reverse transcription kit (Thermo Fisher Scientific, USA). The qRT–PCR mixtures contained the following components: 10 μL of SYBR Green Supermix (TaKaRa, Foster, CA, USA), 0.4 μL of forward primer and reverse primer, 2 μL of cDNA template and 7.2 μL of DEPC water (Sangon, China). The reaction conditions were as follows: 94 °C for 90 s for one cycle; 94 °C for 60 s, 55 °C for 60 s, and 72 °C for 60 s for 40 cycles; and 72 °C for 10 min for one cycle. Finally, the data were normalized to the mRNA level of β-actin, and the target genes were comparatively quantified by the $2^{-\Delta\Delta Ct}$ method. All primers used for quantitative qRT–PCR analysis are listed in Supplemental Table S1.

Multimode ultrasound imaging

A multimode ultrasound imaging system for small animals (Fujifilm Visual Sonics, USA) was used to detect changes in the arterial diameter of the carotid artery after intimal injury in rats. SD rats were anesthetized with isoflurane (MATRX VIP 3000, USA), and signals were collected with a 21 MHz MX series transducer (MX250S) in "M-Mode". Data analyses were performed with FUJIFILM Visual Sonics Measurement software, and the amplitude of vascular pulsation was calculated from the arterial diameters as previously reported [12].

Intracellular ATP measurement

The ATP content was measured with an ATP Assay Kit (Beyotime Biotechnology, China) according to the manufacturer's instructions. Moreover, the ATP values obtained were further standardized to the cell protein concentration.

Analysis of the mitochondrial membrane potential of VSMCs

The mitochondrial membrane potential was assessed with a JC-1 kit (Beyotime Biotechnology, China) according to the manufacturer's instructions. JC-1 accumulates in the matrix of mitochondria at high mitochondrial membrane potential, forming JC1-aggregates, which produces red fluorescence. JC-1 cannot accumulate in the matrix of mitochondria when the mitochondrial membrane potential is low, and JC-1 is a monomer and can produce green fluorescence. In brief, VSMCs were incubated in serum-free medium containing JC-1 (1:1000) for 30 min in the dark at 37 °C, and the nuclei were labeled with a DAPI dilution (1:1000) prepared with PBS. The cells were randomly selected and photographed with a confocal laser microscope.

Analysis of mitochondrial distribution in VSMCs

Mitochondrial morphology was assessed with a MitoTracker Red Kit (Beyotime Biotechnology, China) according to the manufacturer's instructions. Briefly, the VSMCs were incubated with MitoTracker Red-specific fluorescent dyes (1:1000) in the dark at 37 °C for 30 min, and the nuclei were labeled with a DAPI dilution (1:1000) prepared with PBS. The cells were randomly selected and photographed with a confocal laser microscope. The quantification of the mitochondrial distribution was analyzed by Cellsens Dimension software (Olympus Corporation, Shinjuku-ku, Tokyo, Japan). In the software analysis interface, we defined the center of the nucleus as the coordinate origin. Then the coordinates of each red fluorescent signal area (one or more mitochondria combined) were calculated in the cell relative to the origin. According to the coordinates, the mean distance and mean coordinates (absolute value of X, Y) of all red fluorescent areas were calculated in a single cell. Fifteen cells in each group were analyzed and two-tailed Student's t-test was used for statistical analysis.

Mitochondrial DNA copy number measurement

Genomic DNA was extracted with a Rapid Animal Genomic DNA Isolation Kit (Sangon, China) according to the manufacturer's instructions. The relative expression levels of mitochondrial DNA and β-actin mRNA were assessed by qRT–PCR.

Small interfering RNA interference assay

VSMCs were seeded in a six-well plate. After 12–16 h, the confluence of the cells reached 70–80% for the siRNA interference experiments. For RNA interference experiments, PGC1α siRNA or scrambled siRNA (Sangon, China) was transfected with Lipofectamine 2000 in Opti-MEM (Thermo Fisher Scientific, USA) for 48 h. The sequences of the siRNA oligos are listed in Supplemental Table S2.

Frozen sections and hematoxylin/eosin staining

The common carotid arteries of the surgery group and the experimental group were fixed in 4% paraformaldehyde overnight and then dehydrated in 30% sucrose solution for 24 h. After being embedded with embedding agent (Leica, Germany), 8-μm-thick frozen tissue sections were prepared with a frozen slicer (Leica, Germany) and stored at −20 °C.

The frozen sections were removed from −20 °C and rewarmed at room temperature for 30 min. The sections were rinsed with pure water for 1 min, stained with hematoxylin for 8 min, rinsed with pure water for 30 s, dropped into 1% hydrochloric acid ethanol for differentiation for 3–5 s, and rinsed with pure water for termination of differentiation. Basic blue return solution was added for 4 min, and the samples were washed with pure water for 30 s. Photographs were acquired through confocal microscopy (LV1000, Olympus, Japan).

Immunofluorescence staining

The cells were plated on confocal dishes at a density of 1×10^5/well. After washing with PBS, 4% paraformaldehyde was added for fixation for 20 min, and then, 0.3% Triton X-100 was added for 3 min to permeabilize the membrane. After washing with PBS, 10% goat serum was added to the cells, which were blocked at room temperature for

30 min. Then, an anti-PGC1α (1:200, Proteintech, China) primary antibody was added to the cells, which were placed overnight in a refrigerator at 4 °C. On the second day, the secondary antibodies were added to the cells and incubated at room temperature for 2 h. Finally, the nuclei were stained with DAPI at room temperature for 15 min, and fluorescence images were acquired by confocal laser microscopy after washing with PBS.

For blood vessels, frozen sections were rewarmed at room temperature for approximately 30 min, followed by the addition of 0.3% Triton X-100 for 15 min to permeabilize the membrane, washing with PBS for approximately 10 min, and blocking with 10% goat serum at room temperature for 30 min. Then, the sections were incubated with primary antibodies against PGC1α (1:100, Proteintech, China), vWF (1:100, Proteintech, China), and α-SMA (1:100, Proteintech, China) overnight at 4 °C. On the second day, the sections were washed with PBS three times for 5 min each, and the corresponding secondary antibodies were added for incubation at room temperature for 2 h. Finally, the nuclei were stained with DAPI at room temperature for 15 min, and fluorescence images were acquired by laser confocal microscopy.

Drugs

ZLN005 (MCE, USA), a novel PGC1α activator, and SIS3 (MCE, USA), a potent and selective specific Smad3 inhibitor, were used at concentrations of 10 μM and 5 μM, respectively, and were added to the cells 1 h prior to stimulation.

For the in vivo experiment, ZLN005 (2.5 mg/kg) were subcutaneously administered every other day in the rat model of carotid artery injury for four weeks.

Transcriptomic analysis

The arteries with intimal injury were harvested after 4 weeks, and the right carotid arteries without damage were removed for the control, after which RNA sequencing was performed. Briefly, total RNA was extracted from carotid arteries with TRIzol reagent. cDNA libraries were constructed for each pooled RNA sample by VAHTSTM total RNA-seq (H/M/R). Transcript expression analysis of the RNA sequencing was performed by TopHat and Cufflinks [13]. Significance analysis was performed by P value and false discovery rate (FDR) analyses. Differentially expressed genes were analyzed with the DESeq algorithm with the following criteria: fold change > 2 or FDR < 0.05. Gene Ontology (GO) analysis was performed with DAVID Bioinformatics Resources 6.8 (https://david.ncifcrf.gov/) [14]. g: Profiler (https://biit.cs.ut.ee/gprofiler/gost) was used to enrich the biological processes (BPs) of downregulated and upregulated genes identified by RNA sequencing [15]. ClustVis was used to upload raw data and create heatmaps (https://biit.cs.ut.ee/clustvis/). HIPLOT was used to further process the diagram (https://hiplot.com.cn/). REACTOME was used to enrich the BPs of all differentially expressed genes in the RNA sequencing (https://reactome.org/) [16].

Ingenuity pathway analysis

Ingenuity Pathway Analysis (IPA) software (Qiagen) was used to search for genes that are possibly involved in mitochondrial function and predicted the genes upstream of PGC1α through the Grow Tool, which enriched the top significantly changed pathways of downregulated genes identified via RNA sequencing through core analysis. The significance values for analyses of network and pathway generation were calculated with the right-tailed Fisher's exact test by comparing the number of proteins that participate in each function or pathway relative to the total number of occurrences of these proteins in all functional/pathway annotations stored in the Ingenuity Pathway Knowledge Base. IPA was used to understand the complex biological and chemical systems at the core of life science research on the basis of the literature and predicated analysis [17].

Transmission electron microscopy (TEM)

TEM (Talos L120C G2, Thermo Fisher Scientific, Waltham, MA, USA) was used to visualize the ultrastructure of mitochondria in VSMCs. The cells were collected with precooled PBS and treated with 2.5% glutaraldehyde overnight. On the second day, the cells were washed with PBS and fixed in a mixture of 0.8% potassium ferrocyanide and 2% osmium tetroxide in 0.1 M sodium cacodylate buffer for 1 h. Alcohol and epoxy were used for dehydration and embedding, respectively. The slices were observed by TEM. Mitochondrial morphology was analyzed by using CellSens (Olympus, Shinjuku-ku, Tokyo) and ImageJ.

HA-VSMC culture and PGC1α knockout

Human aortic vascular smooth muscle cells (HA-VSMCs) were obtained from Shanghai C-reagent Biotechnology Co. Ltd. Cells were cultured in DMEM containing 10% fetal bovine serum (Gibco, Thermo Fisher Scientific, USA) at 37 °C in 95% air and 5% CO_2. To knock out the PGC1α protein in HA-VSMCs, a lentivirus was applied to the cells with polybrene (5 μg/mL). For the sg-PGC1α lentivirus construction, human PGC1α sgRNA (GenScript, China) was designed and inserted into the pLV[Exp]-Puro-EFS > hCas9:Puro vector (VectorBuilder, China).

HA-VSMCs (MOI = 100) were seeded in six-well plates (2×10^5/well) and infected with lentivirus for 48 h before use.

Untargeted metabolomics analysis

To determine the metabolites of HA-VSMCs under control and PGC1α knockout conditions, HA-VSMCs were washed with precooled PBS, and the cell pellets were quickly frozen in liquid nitrogen before being sent for metabolomics analysis (Suzhou Panomic Biotech Co., Ltd.). For metabolite extraction, 100 mg of glass beads and 1 mL of an acetonitrile: methanol: H_2O mixture (2:2:1) were added to each sample. Then, the mixture was vortexed for 30 s. The mixture was immersed in liquid nitrogen for rapid freezing for 5 min, after which the centrifuge tube was removed and thawed at room temperature. The mixture was ground at 55 Hz for 2 min, and this process was repeated twice. The centrifuge tube was removed, and the mixture was centrifuged for 10 min at 12,000 rpm and 4 °C. The entire supernatant was removed, transferred to a new 2 mL centrifuge tube, concentrated and dried. Three hundred microliters of acetonitrile:2-amino-3-(2-chloro-phenyl)-propionic acid solution prepared with 0.1% formic acid (1:9, V/V) was added accurately to each sample to redissolve it, and the supernatant was filtered through a 0.22 μm membrane and transferred into a detection bottle for LC–MS detection. A Vanquish UHPLC system (Thermo Fisher Scientific, USA) was used for chromatographic separation, and an Orbitrap Exploris 120 (Thermo Fisher Scientific, USA) was used for mass spectrometry acquisition and analysis.

Ropls software was used for all multivariate data analyses and modeling. After the data were scaled, models were built based on orthogonal partial least square discriminant analysis (PLS-DA). P values < 0.05 and VIP values > 1 were considered to indicate statistically significant metabolites. Differentially abundant metabolites were subjected to pathway analysis by MetaboAnalyst, which combines the results from powerful pathway enrichment analysis with those of pathway topology analysis. The metabolites identified via metabolomics were then mapped to the KEGG pathway for biological interpretation of higher-level systemic functions. The metabolites and corresponding pathways were visualized with the KEGG Mapper tool.

Statistical analysis

Statistical analysis was performed, and figures were prepared with GraphPad Prism 8.0 (GraphPad Software, CA). Each experiment in this study was replicated at least 4 times, and all the data are presented as the mean ± standard deviation (*SD*). For comparisons of data from fewer than 30 samples, nonparametric tests were used. A two-tailed Mann–Whitney test was used for comparisons between two groups, and $P < 0.05$ was considered statistically significant. Nonparametric tests were used.

Results

Mitochondrial dysfunction contributes to neointimal proliferation

To investigate the mechanism of VSMC hyperproliferation after intimal injury, we established a rat intimal injury model to investigate mitochondrial morphology in a rodent model. The left common carotid artery of each rat was used as the injured group, and the right common carotid artery was used as the autologous control group. HE staining revealed that the VSMCs excessively proliferated with significant intimal hyperplasia at 4 weeks after injury (Fig. 1A). We subsequently performed RNA sequencing analysis (GSE285663) to explore the transcriptomic changes. The volcano plot revealed that 8,351 genes were downregulated and that 9,397 genes were upregulated in the injured group compared with the control group (Fig. 1B). The Gene Ontology (GO) cellular component (CC) analysis revealed that 32% of the downregulated genes were in the 'Cytoplasm' category, 28% were in the 'Nucleus' category, and 18% were in the 'Mitochondria' category (Fig. 1C). The database enrichment analysis of the upregulated genes revealed that the majority were predominantly localized in the cytoplasm, with no significant enrichment in mitochondria-related pathways (Supplemental Fig. 1). To investigate the pathways involved, we used IPA to enrich the biological pathways of the downregulated genes. The results revealed that energy metabolism, such as OXPHOS, significantly changed in intimal injured rats and that mitochondrial dysfunction was the most obvious feature of intimal injury, indicating the important role of mitochondria (Fig. 1D). To assess mitochondrial function, we first assessed mitochondrial morphology. Transmission electron microscopy (TEM) revealed that the roundness of the mitochondria significantly increased, but the number of mitochondria decreased after injury. Moreover, the mitochondrial cristae of the injured carotid artery were damaged (Fig. 1E). Similarly, we observed that the mitochondrial cristae in both the carotid plaque and the femoral artery plaque were also damaged in the samples obtained from patients who underwent endarterectomy (Fig. 1F).

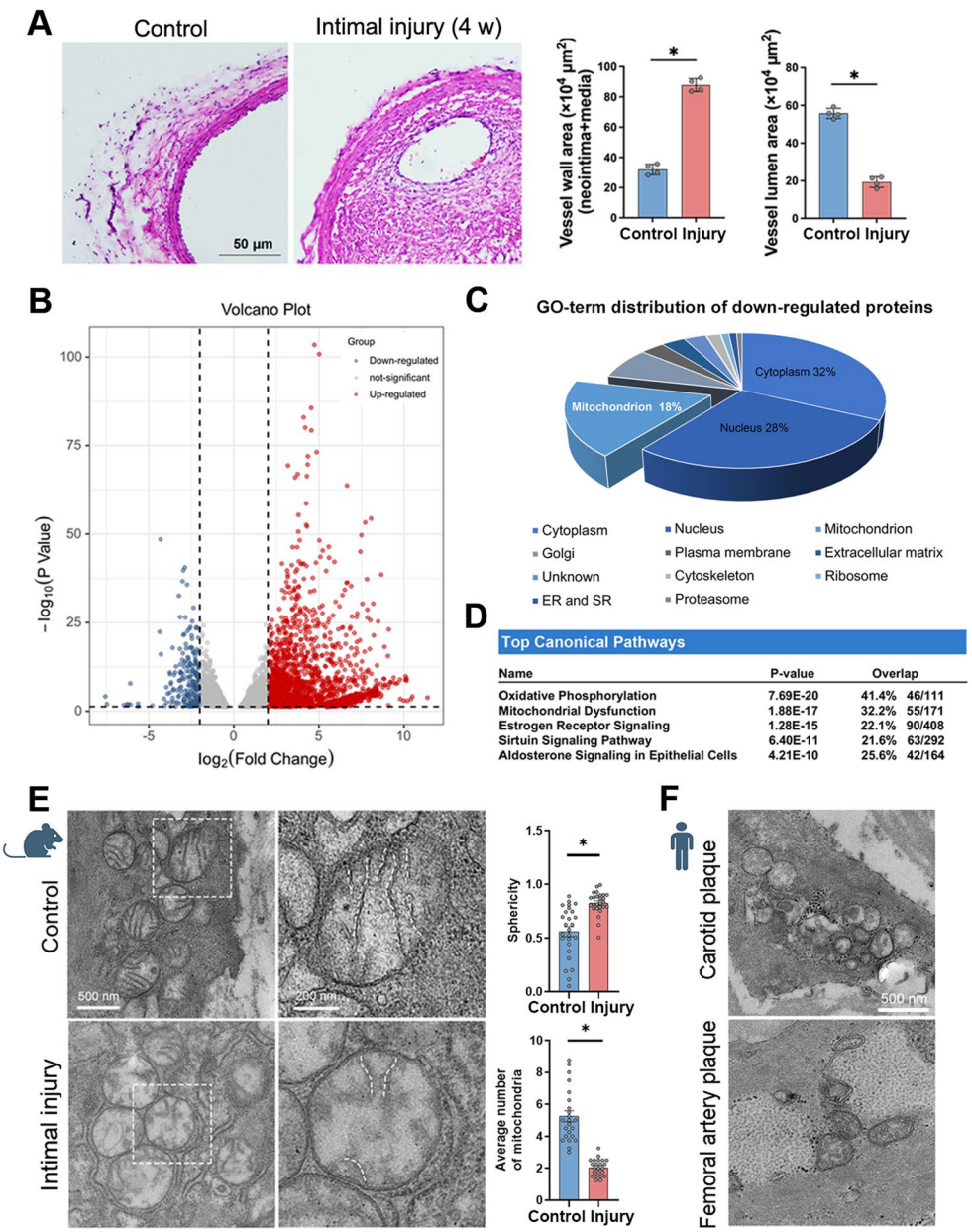

Fig. 1 Mitochondrial dysfunction contributes to neointimal hyperplasia of the injured carotid artery. (**A**) Representative HE-stained images of the carotid artery on the control side and injured side at 4 weeks postinjury. The areas of the arterial neointima and lumen were analyzed by ImageJ ($n=4$). Scale bar = 50 μm. (**B**) Volcano plots of differential gene expression by RNA sequencing analysis of the 4-week intimal injury rat model. (**C**) A pie graph of the GO term distribution of downregulated proteins in the injured group compared with the control group. GO cellular component analysis revealed that 32% of the downregulated genes were in the 'Cytoplasm' category, 28% were in the 'Nucleus' category, and 18% were in the 'Mitochondria' category. (**D**) Graph depicting the top 5 significantly changed pathways ($P<0.01$) derived from an IPA analysis of the significantly downregulated proteins. Mitochondrial dysfunction was significantly altered. (**E**) Representative images of the mitochondrial ultrastructures of control vessels and vessels with intimal injury acquired by TEM ($n=26$ mitochondria). Scale bar, 500 nm for the left figures and 200 nm for the right figures. (**F**) Representative ultrastructural images of the mitochondria of the human carotid plaque and the femoral artery plaque by TEM. Scale bar = 500 nm. *P* values were calculated by a two-tailed Mann–Whitney test. The values are shown as the means ± *SD*. * $P<0.05$

Physiological cyclic stretch in vitro promotes VSMC mitochondrial function

To explore the effect of mechanical stretch on VSMC hyperproliferation, multimodal ultrasound imaging of small animals was used to determine the amplitude of vascular pulsation in the injured left carotid arteries and the untreated self-control. Four weeks after injury, the average pulsation amplitude of the injured vessel was 3.44%; in contrast, the average amplitude in the uninjured group was approximately 14.98%, with the difference between the two group being 11.54 ± 1.542% (Fig. 2A). Therefore, we used static conditions to mimic the injured group and cyclic stretch at a magnitude of 10% to mimic the uninjured group in in vitro experiments (Fig. 2B). To further verify the consistency of mitochondrial function changes in VSMCs in vivo and in vitro, VSMCs were subjected to cyclic stretch for 24 h at 10% amplitude and 1.25 Hz frequency by a FX-5000T instrument to simulate physiological conditions (CS), and the VSMCs without cyclic stretch loading were used as the static control group (ST).

The distribution of mitochondria was detected by MitoTracker Red, a mitochondria-specific fluorescent probe. To confirm its specificity, the morphology of mitochondria was analyzed by MitoTracker Red staining with 100x magnification using structured illumination microscopy. It indicated that only negligible red signals from other membrane structures were observed (Supplemental Fig. 2A). Hence,

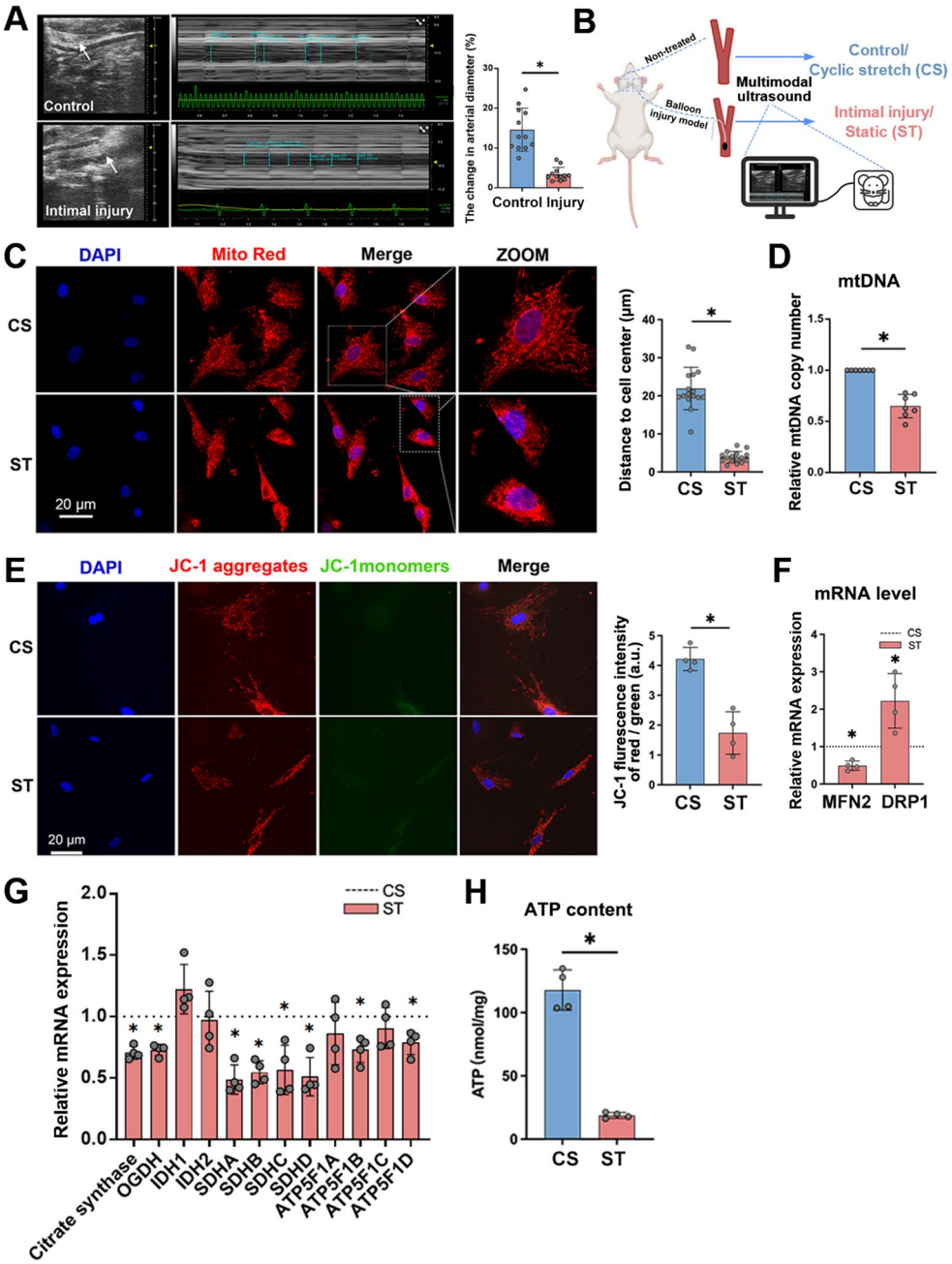

Fig. 2 Physiological cyclic stretch (CS) increased VSMC mitochondrial mass and ATP production in vitro. (**A**) Representative ultrasound images of the carotid artery on the self-control side and injured side at 4 weeks postinjury were used to measure the change in the carotid arterial inner diameter ($n=4$). (**B**) Flow chart depicting the process of multimode ultrasound imaging in the intimal injury model. In an in vitro study, cyclic stretch (CS) mimicked the control group in vivo, and the static condition (ST) mimicked the in vivo injury group. (**C**) Representative immunofluorescence images of the distribution of mitochondria (red) ($n=16$). Blue: DAPI; scale bar = 20 μm. (**D**) mtDNA levels were determined by qRT–PCR ($n=6$). (**E**) Representative immunofluorescence images of JC-1 staining used to determine the membrane potential of mitochondria ($n=4$). Blue: DAPI; red: JC-1 aggregates; green: JC-1 monomers. Scale bar = 20 μm. (**F**) MFN2 and DRP1 mRNA levels were determined by qRT–PCR ($n=4$). (**G**) VSMC mRNA levels of key rate-limiting enzymes in the mitochondrial function pathway were determined by qRT–PCR ($n=4$). (**H**) ATP content was determined by a luciferase assay system ($n=4$). *P* values were calculated by a two-tailed Mann–Whitney test. The values are shown as the means ± *SD*. * $P<0.05$

MitoTracker Red was utilized to delineate mitochondrial morphology and determine the intracellular localization of mitochondria in the present study. Compared with that in the static group, the distribution of mitochondria changed from a perinuclear aggregate distribution to a loose cytoplasmic distribution under physiological cyclic stretch (Fig. 2C). To exclude the possibility that changes in the distance between mitochondria and the nucleus might be attributed to alterations in cell size, we measured the cell area of VSMCs in both the CS and ST groups using F-actin staining. The results revealed no significant differences in cell size between the two groups (Supplemental Fig. 2B). The mitochondrial DNA (mtDNA) copy number and ATP synthesis were significantly increased in the VSMCs subjected to cyclic stretch (Fig. 2D and H), which suggested that cyclic stretch promoted mitochondrial energy metabolism functions. The membrane potential of the mitochondria was determined with a JC-1 probe. Compared with that in the cyclic stretch group, the mitochondrial membrane potential was decreased under static conditions (Fig. 2E). In addition, compared with that in the cyclic stretch group, the mRNA expression of MFN2 was decreased, whereas that of dynamin-related protein 1 (DRP1) was increased under static conditions (Fig. 2F), suggesting that mitochondrial

dynamics changed toward fusion by cyclic stretch. The key rate-limiting step enzymes involved in the TCA cycle were assessed by qRT–PCR. Among the twelve genes related to mitochondrial function, the expression of mainly mitochondrial genes, including citrate synthase, OGDH, SDHA, SDHB, SDHC, SDHD, ATPF1B and ATPF1D, in VSMCs significantly decreased without cyclic stretch (Fig. 2G). These results indicated that the mitochondrial function of VSMCs was the most significantly altered metabolic pathway upon physiological cyclic stretch stimulation in vitro, which was consistent with the in vivo RNA sequencing results.

Physiological cyclic stretch increases PGC1α expression in VSMCs

To further investigate the key regulators of the mitochondrial function of VSMCs, we analyzed the downregulated genes distributed in the mitochondria in Fig. 1C by the GO (Fig. 3A), KEGG and REACTOME (Fig. 3B) databases. We found that most of the biological pathways were classified as mitochondrial biosynthesis and energy metabolism pathways, such as OXPHOS, the electron transport chain (ETC) and ATP synthesis. Therefore, we selected the PPARγ coactivator 1 (PGC1) family, which are transcription coactivators that include PGC1α and PGC1β, for further exploration. They are key molecules in mitochondrial biosynthesis and regulate genes involved in energy metabolism [5]. Then, we used IPA to connect PGC1α and PGC1β with different mitochondrial function processes and found that PGC1α was more closely related to mitochondrial function (Fig. 3C). We first assessed the mRNA levels of PGC1α and PGC1β by qRT–PCR, and the results indicated that the mRNA levels of PGC1α were significantly regulated by mechanical stretch (Fig. 3D). The protein levels of PGC1α were significantly increased by cyclic stretch compared with those of the static group (Fig. 3E). In addition, the mRNA expression of PGC1α downstream target genes (ESRRA and NRF1) were also significantly increased by cyclic stretch, indicating that PGC1α could effectively trigger the transcription of its downstream target genes (Supplemental Fig. 3A). Moreover, consistent with the results from the subcellular localization of PGC1α in UniProt (Supplemental Fig. 3B), an immunofluorescence assay and cytoplasmic separation revealed that PGC1α was localized mainly in the cytoplasm of VSMCs and was upregulated by mechanical stretch (Fig. 3F and G). Taken together, these data indicated that PGC1α, which is closely related to mitochondrial function, in VSMCs was significantly increased upon physiological cyclic stretch stimulation.

Activation of PGC1α significantly facilitates mitochondrial function in VSMCs

To explore the role of PGC1α in VSMC mitochondrial function, we applied a specific activator of PGC1α, ZLN005, in subsequent experiments. VSMCs were treated with 10 μM ZLN005 for 0, 12, 24, or 48 h. The western blot results revealed that an incubation time of 48 h was effective (Supplemental Fig. 3 C). Hence, ZLN005 treatment at 10 μM for 48 h was used as the subsequent experimental condition. Compared with that in the negative control group (NC), the protein expression of PGC1α in VSMCs was strongly increased under ZLN005 stimulation (Fig. 4A), as was the mRNA expression of PGC1α and its downstream target genes (ESRRA and NRF1) (Supplemental Figs. 3D and E). The copy number of mitochondrial DNA and ATP synthesis were also significantly increased after ZLN005 treatment (Fig. 4B and F), suggesting that the activation of PGC1α upregulated mitochondrial energy metabolism functions. MitoTracker Red staining revealed that compared with that in the NC group, the distribution of mitochondria changed from a perinuclear aggregate distribution to a loose cytoplasmic distribution after ZLN005 treatment (Fig. 4C). Compared with that in the control group, the mRNA expression of MFN2 was significantly increased, whereas the mRNA expression of DRP1 was significantly decreased (Fig. 4D), indicating that ZLN005 affected mitochondrial dynamics toward mitochondrial fusion. JC-1 staining revealed that, compared with that in the control group, the mitochondrial membrane potential was also increased by ZLN005 (Fig. 4E).

To further verify the effect of PGC1α, VSMCs were transfected with PGC1α-specific small interfering RNA (siRNA) or scrambled siRNA. Compared with the scrambled siRNA, siRNA3 had the most obvious interference effect, and the mRNA and protein expression levels of PGC1α were significantly lower (Supplemental Figs. 3 F, G and G). In addition, the mRNA expression of PGC1α downstream target genes was also significantly inhibited (Supplemental Fig. 3H). Similarly, functional changes in mitochondria were explored under PGC1α interference conditions. The mitochondrial DNA copy number and ATP synthesis were also markedly decreased by PGC1α knockdown (Fig. 4H and L), indicating that the repression of PGC1α downregulated mitochondrial energy metabolism functions. Moreover, MitoTracker Red staining revealed that the distribution of mitochondria changed from a loose cytoplasmic distribution to perinuclear aggregation in response to PGC1α siRNA upon CS (Fig. 4I). The mRNA expression level of MFN2 was significantly decreased, whereas that of DRP1 was strongly increased by PGC1α siRNA (Fig. 4J), suggesting that the downregulation of PGC1α induced

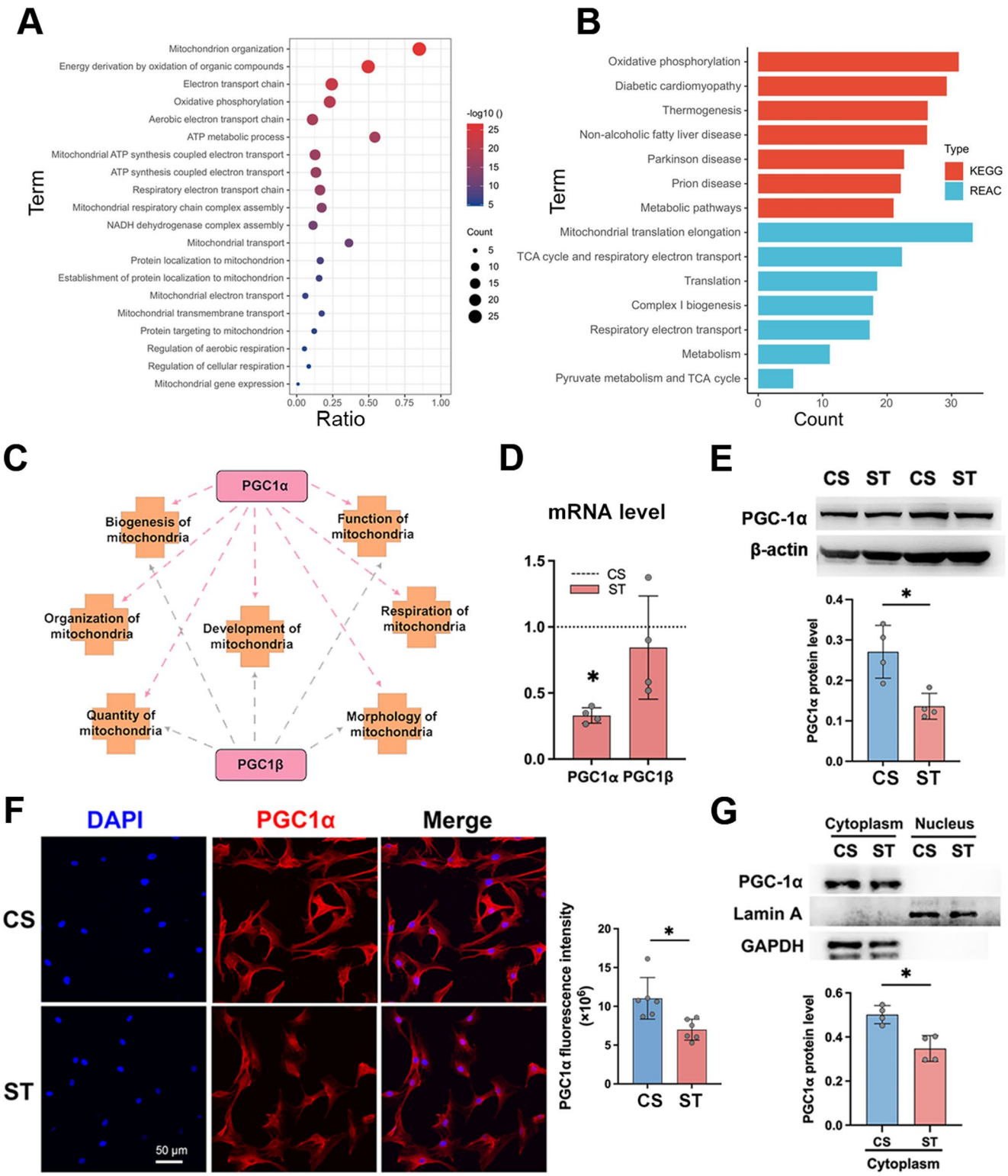

Fig. 3 Physiological cyclic stretch increased PGC1α expression in VSMCs in vitro. (**A**) GO enrichment analysis of proteins significantly downregulated in mitochondria. (**B**) KEGG and REACTOME enrichment analysis of significantly downregulated proteins from mitochondria. (**C**) Associations between PGC1α and PGC1β and multiple mitochondrial functions according to IPA. (**D**) The mRNA levels of PGC1α and PGC1β were determined by qRT–PCR ($n=4$). (**E**) The protein level of PGC1α determined by western blot under CS and ST conditions ($n=4$). (**F**) Representative immunofluorescence images of PGC1 under CS and ST conditions. Scale bar = 50 μm. (**G**) The protein level of PGC1α in the cytoplasm and nucleus was determined by western blotting ($n=4$). *P* values were calculated by a two-tailed Mann–Whitney test. The values are the means ± *SD*. * $P<0.05$

mitochondrial fission in VSMCs. JC-1 staining revealed that the mitochondrial membrane potential was also reduced by PGC1α knockdown (Fig. 4K).

These observations suggested that mitochondrial function was positively correlated with the expression of PGC1α and its downstream targets, which prompted us to further investigate the underlying mechanism by which PGC1α regulates mitochondrial function in VSMCs.

PGC1α knockout in human aortic VSMCs impairs mitochondrial metabolism

To further verify the role of PGC1α in mitochondrial energy metabolism in human cells, we knocked out PGC1α in HA-VSMCs. The knockout efficiency of PGC1α was demonstrated in Supplemental Fig. 4. TEM analysis revealed that the mitochondrial cristae were obviously damaged in the PGC1α knockout group (Fig. 5A). To determine the mitochondrial morphology and number of HA-VSMCs, we used MitoTracker Red to label mitochondria and obtained microscopy images via 3D-structured illumination microscopy. We detected a significant decrease in the number of mitochondria in the PGC1α-knockout group (Fig. 5B). We used untargeted metabolomic studies to further investigate the mitochondria-associated changes in metabolites in HA-VSMCs under control and knockout conditions. PLS-DA revealed that the control group and the PGC1α knockout group were relatively clustered, indicating that the metabolomics results of this study were relatively reliable (Fig. 5C). By hierarchical clustering of differentially abundant metabolites, we found that most of the differentially abundant metabolites in the PGC1α knockout group were significantly downregulated (Fig. 5D). By KEGG enrichment analysis of these differentially abundant metabolites, we found that the TCA cycle was an enriched pathway and was downregulated (Fig. 5E). These results further confirmed that mitochondrial energy metabolism was inhibited when PGC1 was downregulated in human cells.

Smad3 regulates VSMC mitochondrial function by interacting with PGC1α and regulating its expression

PGC1α is regulated by AMPK [18] and SIRT1 [19]. To identify the novel regulatory mechanism, first, the first 100 molecules that directly regulate PGC1α were identified through IPA (Fig. 6A). We then compared the genes that participated in the pathways and cell functions related to cardiovascular disease by Venn diagram comparison and identified eight genes that were in common (Fig. 6B). The 8 upstream molecules of PGC1α are PPARG, PPARD, PPARA, SMAD3, SIRT1, TP53, NR1H4 and CEBPB. After associating these 8 genes with cardiovascular disease-related functions, Smad3 was selected for further study (Fig. 6C).

Western blot results showed that cyclic stretch significantly induced the phosphorylation level of Smad3 at 6 h, whereas which did not significantly change at 24 h (Fig. 6D and E). Notably, the total Smad3 levels did not significantly change at 6 h and 24 h after cyclic stretch, suggesting that the phosphorylation of Smad3, an upstream regulator of PGC1α, is an early response to mechanical stimulation. To further explore the regulatory relationship between Smad3 and PGC1α, a specific phosphorylation inhibitor of Smad3, SIS3, was used. Compared with the negative control, SIS3 inhibited the phosphorylation of Smad3; moreover, the expression of PGC1α and mtDNA copy number were also significantly decreased by SIS3 under static conditions and cyclic stretch (Fig. 6F and G). These results indicated that cyclic stretch enhanced the phosphorylation of Smad3, which upregulated the expression of PGC1α, further enhancing mitochondrial biogenesis.

Intimal injury represses PGC1α expression in vivo

By using a rat intimal injury model, we verified the role of PGC1α in regulating mitochondrial function in vivo. The results of PGC1α immunofluorescence staining suggested that PGC1α expression was decreased in the injured vessel (Fig. 7A). The mRNA and protein levels of PGC1α were strongly decreased (Fig. 7B and C). The mRNA expression of the PGC1α downstream target genes PPARA, PPARD and ESRRA was also significantly reduced (Fig. 7D). In addition, MFN2 mRNA expression in injured vessels decreased significantly, whereas DRP1 mRNA levels increased significantly, indicating the occurrence of mitochondrial fission (Fig. 7E). We also examined the RNA-seq results of the rat intimal injury model and generated a heatmap including the rate-limiting step enzymes in energy metabolism (Fig. 7F), and the qRT–PCR results revealed that the mRNA levels of HK2, CPT1A, CPT1B, citrate synthase, OGDH, SDHA, SDHB, SDHC, SDHD, ATPF1B, and ATPF1D were significantly changed in the injured vessel (Fig. 7G). These data suggested that the expression of PGC1α was decreased and that mitochondrial functions, including mitochondrial biogenesis, mitochondrial dynamics, and the key mitochondrial rate-limiting step enzymes involved in mitochondrial energy metabolism functions, were impaired after intimal injury.

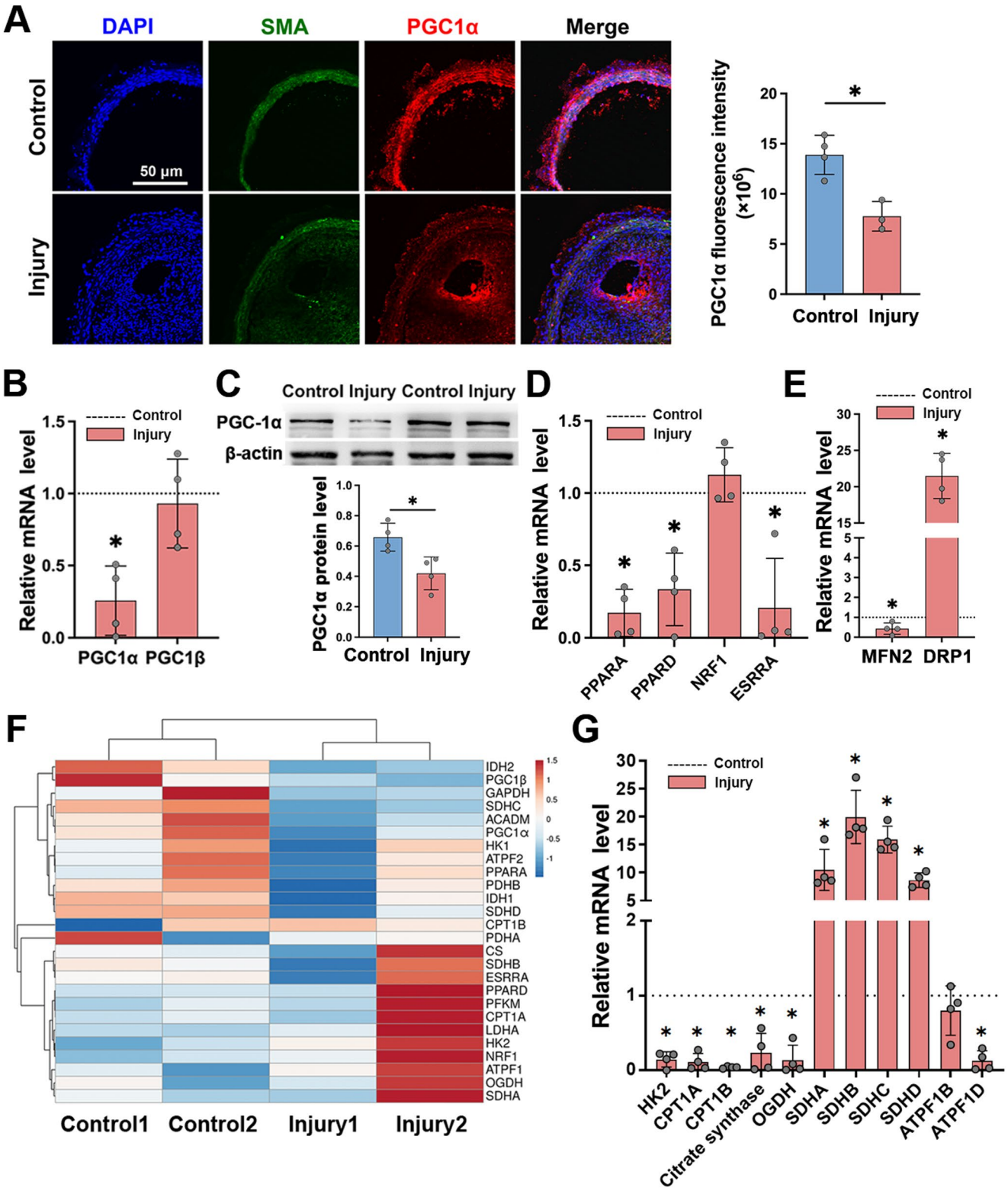

The specific PGC1α activator ZLN005 enhances mitochondrial function and inhibits neointimal hyperplasia in an intimal injury model

To investigate treatments that inhibit neointimal hyperproliferation, we subcutaneously injected the PGC1α activator ZLN005 every other day into 4-week intimal injury model rats to further evaluate the association between PGC1α and

Fig. 4 The PGC1α activator ZLN005 promoted VSMC mitochondrial function, but siRNA targeting PGC1α inhibited VSMC mitochondrial function. (**A**) The protein level of PGC1α determined by western blot under control and ZLN005 (10 μM) conditions for 48 h ($n=5$). (**B**) The mRNA level of mtDNA after treatment with ZLN005 was determined by qRT–PCR ($n=5$). (**C**) Representative immunofluorescence images of the distribution of mitochondria (red) in VSMCs after treatment with ZLN005 ($n=15$). Blue: DAPI; scale bar = 20 μm. (**D**) The mRNA levels of MFN2 and DRP1 after treatment with ZLN005 were determined by qRT–PCR ($n=4$). (**E**) Representative immunofluorescence images of JC-1 staining used to determine the membrane potential of mitochondria after treatment with ZLN005 ($n=4$). Blue: DAPI; red: JC-1 aggregates; green: JC-1 monomers. Scale bar = 20 μm. (**F**) ATP production was determined by a luciferase assay after treatment with ZLN005 ($n=4$). (**G**) The protein level of PGC1α in VSMCs treated with siRNA was determined by western blotting ($n=5$). (**H**) The mRNA level of mtDNA after siRNA treatment was determined by qRT–PCR ($n=4$). (**I**) Representative immunofluorescence images of the distribution of mitochondria after siRNA treatment ($n=15$). Blue: DAPI; red: MitoTracker Red. Scale bar = 20 μm. (**J**) The mRNA levels of MFN2 and DRP1 in VSMCs treated with siRNAs were determined by qRT–PCR ($n=4$). (**K**) Representative immunofluorescence images of JC-1 staining used to determine the membrane potential of mitochondria after siRNA treatment ($n=4$). Blue: DAPI; red: JC-1 aggregates; green: JC-1 monomers. Scale bar = 20 μm. () ATP content in VSMCs transfected with siRNA was determined by a luciferase assay system ($n=4$). *P* values were calculated by a two-tailed Mann–Whitney test. The values are shown as the means ± *SD*. * $P<0.05$

mitochondrial function in vivo (Fig. 8A). To determine the optimal concentration of ZLN005, preliminary experiments revealed that both low and high doses of ZLN005 significantly enhanced PGC1α transcriptional levels (Supplemental Fig. 5). Considering the potential biotoxicity of ZLN005 and the long-term nature of the four weeks experiment, a dose of 2.5 mg/kg was selected for subcutaneous injection in subsequent experiments. First, we assessed the expression of PGC1α mRNA and protein, which was significantly increased by ZLN005 treatment (Fig. 8B and C). Immunofluorescence staining of PGC1α also revealed that the expression of PGC1α was increased by ZLN005 (Fig. 8D). The mRNA abundance of rate-limiting step enzymes involved in energy metabolism, including CPT1B, SDHA, SDHC, SDHD, ATPF1B, and ATPF1D, increased with ZLN005 treatment (Fig. 8E). Moreover, the mRNA levels of PGC1α downstream target genes were also significantly increased by ZLN005 (Fig. 8F). HE staining revealed that injury animals treated with ZLN005 presented significantly less neointimal hyperproliferation, indicating greater vascular patency (Fig. 8G). These data suggested that ZLN005, a specific activator of PGC1α, effectively alleviated mitochondrial dysfunction by increasing the expression of PGC1α, which ultimately inhibited VSMC hyperproliferation after intimal injury but promoted mitochondrial biosynthesis, mitochondrial dynamics, and the key rate-limiting step enzymes involved in mitochondrial energy metabolism functions.

Discussion

In this study, our results demonstrated that physiological mechanical stretch promotes PGC1α for regulating mitochondrial functions via p-Smad3 in vitro and that the activation of PGC1α prevents neointimal hyperplasia by enhancing mitochondrial function after intimal injury in vivo. This mechanism is based on the following findings: (1) an abnormal ultrastructure of mitochondria occurred in human plaques and murine neointimal hyperplasia, and metabolic dysfunction, especially mitochondrial dysfunction, was found in the 4-week rat intimal injury model; (2) the injured vessel had a lower fluctuating amplitude, indicating a significant change in the hemodynamic force; (3) in vitro, physiological cyclic stretch upregulated VSMC PGC1α expression, mitochondrial biogenesis, mitochondrial fusion, and mitochondrial energy metabolism; and (4) importantly, the PGC1α-specific activator ZLN005 enhanced mitochondrial metabolism, which effectively inhibited VSMC hyperproliferation in vivo. Overall, these data demonstrate the importance of mechanical stretch in regulating PGC1α and mitochondrial metabolism in VSMCs, which are essential for inhibiting neointimal hyperplasia both in vitro and in vivo.

Neointimal hyperplasia often occurs in the early stage of cardiovascular disease [20, 21]. VSMCs are the main components of neointimal hyperplasia under pathological conditions. Importantly, VSMCs are primarily subjected to cyclic stretch resulting from pulsatile blood pressure [22], and changes in hemodynamics strongly influence VSMC function [23, 24]. Therefore, it is vital to explore the role of mechanical stretch in the process of neointimal hyperplasia. Hence, we established a vascular injury animal model in vivo and applied cyclic stretch by the Flexcell-5000T system in vitro. We found that the circumferential strain of the injured side carotid artery was approximately 3.44%, while that of the control side was about 14.98%, resulting in a difference of 11.54 ± 1.542% after intimal injury, indicating that the VSMCs were exposed to less mechanical stretch during the process of neointimal hyperplasia in vivo. To simulate the changes, we used a static condition to mimic the injured arteries and applied 10% cyclic stretch to represent the control arteries in vivo. Cyclic stretch has been reported to increase mitochondrial mass and ATP production in a cultured cardiac cell line [25]. Our results indicated that physiological CS promotes mtDNA copy number, mitochondrial membrane potential and ATP production in VSMCs. All of them influence mitochondrial function, and PGC1α, an important transcriptional coactivator, participates in regulating mitochondrial function in response to mechanical stretch.

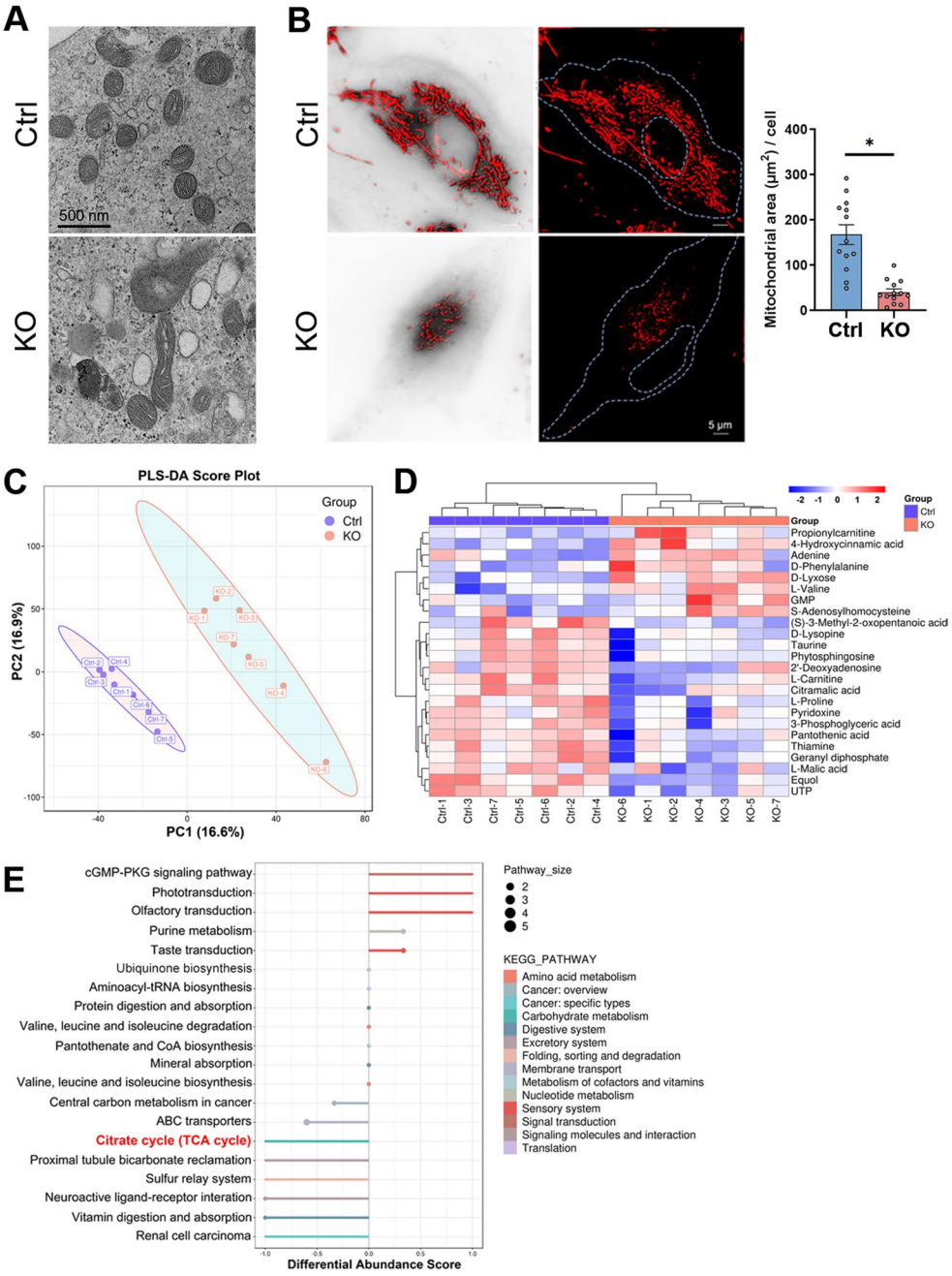

Fig. 5 PGC1α knockout repressed mitochondrial function in human aortic VSMCs. (**A**) The ultrastructures of control and PGC1α knockout human aortic VSMC mitochondria were visualized by TEM. Scale bar = 500 nm. (**B**) Representative immunofluorescence images of human aortic VSMC mitochondria labeled with MitoTracker Red acquired by 3D-structured illumination microscopy ($n = 13$). Scale bar = 5 μm. (C) PLS-DA score plot of the untargeted metabolomics study. (**D**) Hierarchical clustering heatmaps of differentially abundant metabolites identified via metabolomics analysis between the control group and the PGC1α knockout group. (**E**) Differential enrichment score map of the metabolomics. *P* values were calculated by a two-tailed Mann–Whitney test. The values are shown as the means ± *SD*. * $P < 0.05$

Mitochondrial function is closely related to the proliferation, migration, and phenotypic transformation of VSMCs [26, 27], whereas mitochondrial dysfunction is accompanied by an imbalance in energy metabolism [28]. For example, in hypertensive mice, VSMCs exhibit a synthetic phenotype of overproliferation and mitochondrial dysfunction [29]. In a study of pulmonary hypertension (PAH), mitochondrial fission in pulmonary artery smooth muscle cells (PASMCs) was demonstrated to play a key role in the process of excessive proliferation [27]. Inhibition of DRP1 or activation of MFN1 and MFN2 by mitochondrial mitogenic inhibitor 1 (Mdivi-1) can inhibit PASMC proliferation, thus effectively alleviating the disease. Ca^{2+}/calmodulin-dependent protein kinase II (CaMKII) is an important molecule involved in the mitochondrial uptake of Ca^{2+}, which can be enhanced by mitochondrial motility, and promotes the migration and proliferation of VSMCs [30]. Thus, the inhibition of CaMKII could effectively reduce neointimal hyperplasia after vascular injury. Mitochondria also play a key role in the generation of reactive oxygen species (ROS), which are important mediators involved in the proliferation and migration of VSMCs [31, 32]. Taken together, these observations suggest that mitochondria play an important role in regulating VSMC function and that targeting mitochondrial function

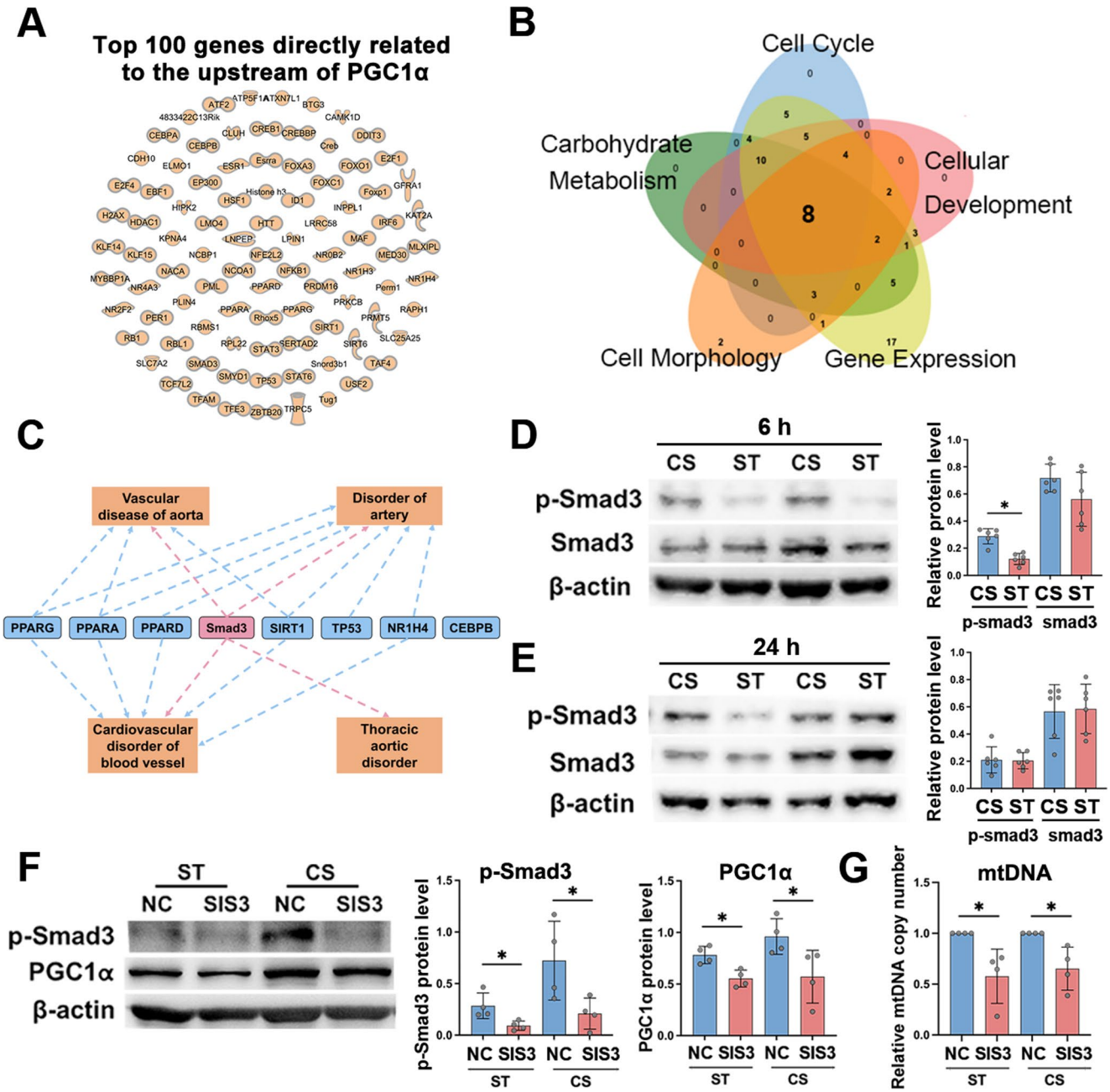

Fig. 6 Smad3 regulated mitochondrial function by regulating PGC1α in response to CS. (**A**) Top 100 genes directly related to genes upstream of PGC1α as predicted by IPA. (**B**) Venn diagram comparison of genes from five pathways related to molecular and cellular functions; eight genes, including PPARG, PPARA, PPARD, SMAD3, SIRT1, TP53, NR1H4 and CEBPB, overlapped. (**C**) Eight target molecules (blue and pink) were associated with four molecular functions closely related to cardiovascular disease (orange regions). (**D**, **E**) The protein levels of p-Smad3 and Smad3 in VSMCs treated with CS for 6–24 h were determined by western blotting ($n=6$). (**F**) The protein levels of PGC1α and p-Smad3 in VSMCs treated with SIS3 ($n=4$). (**G**) The mRNA level of mtDNA in VSMCs treated with SIS3 was determined by qRT–PCR ($n=4$). *P* values were calculated by a two-tailed Mann–Whitney test. The values are the means ± *SD*. * $P<0.05$

is a potential therapeutic strategy for treating neointimal hyperplasia.

PGC1α has been identified as a major transcriptional regulator of cellular metabolism [33, 34]. PGC1α dysregulation represents metabolic disorders in the body and is considered a potential target molecule for most metabolic diseases [35, 36]. In thoracic aortic aneurysms, abnormally low expression of PGC1α is associated with excessive ROS and severe mitochondrial dysfunction [37]. In general, PGC1α is activated by AMPK and SIRT1 to reduce ROS levels and can increase the level of mitochondria [10, 38, 39]. PGC1α is required for endothelial flow alignment in vitro and in vivo

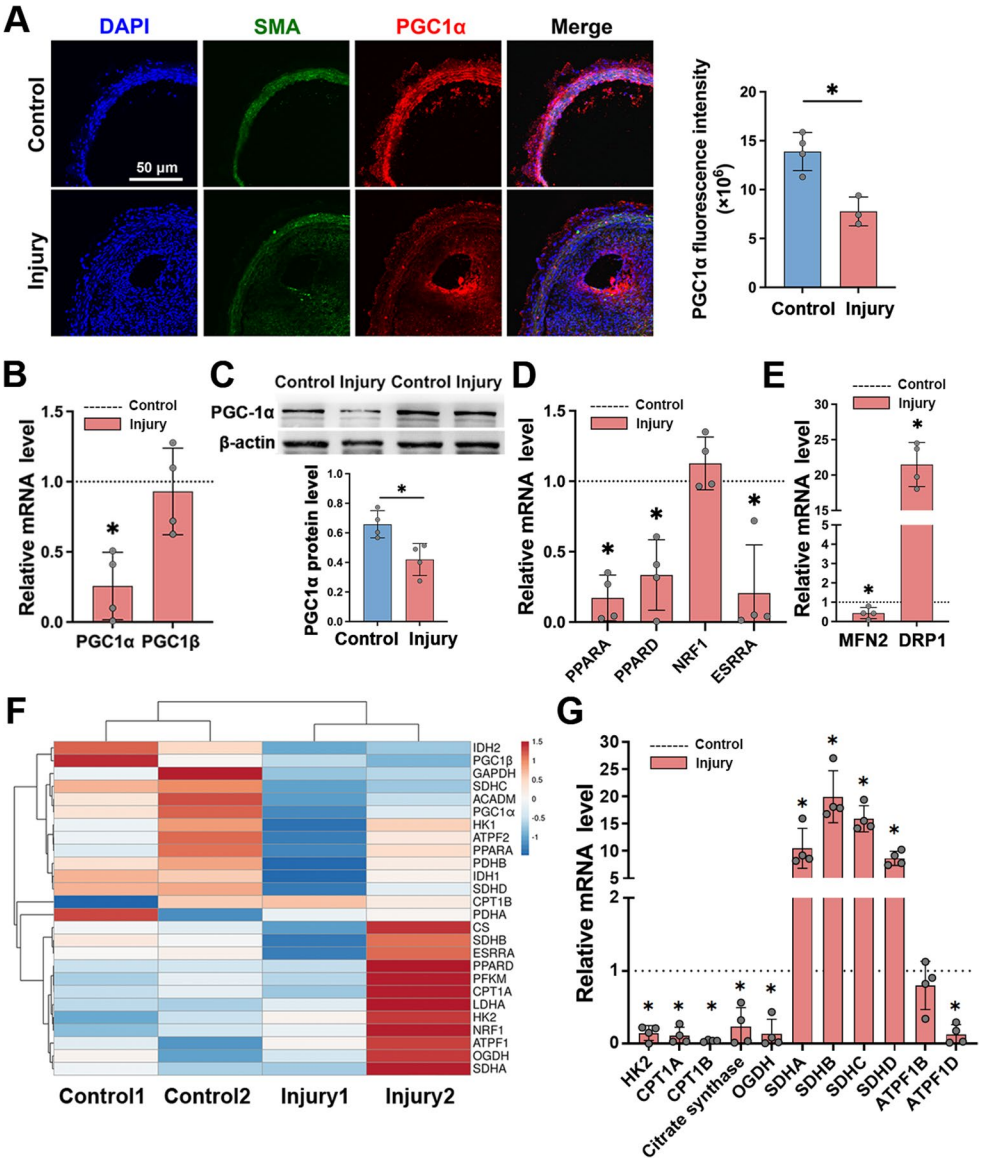

Fig. 7 Intimal injury impaired mitochondrial function and inhibited PGC1α expression in vivo. (**A**) Representative immunofluorescence images of the carotid artery on the control side and injured side at 4 weeks ($n \geq 3$). Blue: DAPI; green: SMA; red: PGC1α. Scale bar = 50 μm. (**B**) The mRNA levels of PGC1α and PGC1β in the carotid artery on the injured side compared with those on the control side were determined by qRT–PCR ($n = 4$). (**C**) The protein level of PGC1α in the carotid artery on the control side and injured side was determined by western blotting ($n = 4$). (**D**) The mRNA levels of PGC1α target genes in the carotid artery on the injured side compared with those on the control side were determined by qRT–PCR ($n = 4$). (**E**) The mRNA levels of MFN2 and DRP1 of carotid artery on the injured side compared with those on the control side were determined by qRT–PCR ($n = 4$). (**F**) Heatmap of the fold change in the expression of rate-limiting enzymes involved in energy metabolism according to the RNA-seq results of the arteries with intimal injury at 4 weeks. (**G**) The mRNA levels of rate-limiting enzymes in the carotid artery on the injured side compared with those on the control side were determined by qRT–PCR ($n = 4$). *P* values were calculated by a two-tailed Mann–Whitney test. The values are shown as the means ± *SD*. * $P < 0.05$

while stabilizing the endothelium and rendering it resistant to atherosclerosis and thrombosis [40]. ZLN005 was firstly used as a novel small molecular to increase PGC1α gene transcription in skeletal muscle, and improve the glucose tolerance, pyruvate tolerance, and insulin sensitivity of diabetic db/db mice [41].Restoring PGC1α activity with PGC1α activator ZLN005 increased radiosensitivity of resistant glioma cells by reactivating mitochondria-related reactive oxygen species production and inducing apoptotic effects both in vitro and in vivo [42].

In our study, physiological CS upregulated the expression of PGC1α, mitochondrial biogenesis and energy metabolism. In addition, after activation or repression of PGC1α by the specific activator ZLN005 or by the PGC1α siRNA, respectively, changes in mitochondrial function were observed according to changes of mitochondrial DNA copy number, mitochondrial membrane potential and ATP production. Moreover, in the 4-week intimal injury model, VSMCs overproliferated, and PGC1α expression was significantly downregulated, accompanied by a decrease in mitochondrial dysfunction. In contrast, stimulation with the PGC1α-specific activator ZLN005 in vivo effectively relieved the excessive proliferation of VSMCs and promoted the repair of intimal injury. These results suggested that PGC1α promoted mitochondrial function both in vivo and in vitro, including mitochondrial biogenesis, mitochondrial dynamics, and the key mitochondrial rate-limiting step enzymes involved in the three main energy metabolism pathways in VSMCs, namely, the citric acid cycle, respiratory electron transfer chain and ATP synthesis.

We further explored the specific mechanism by which PGC1α regulates mitochondrial function through its

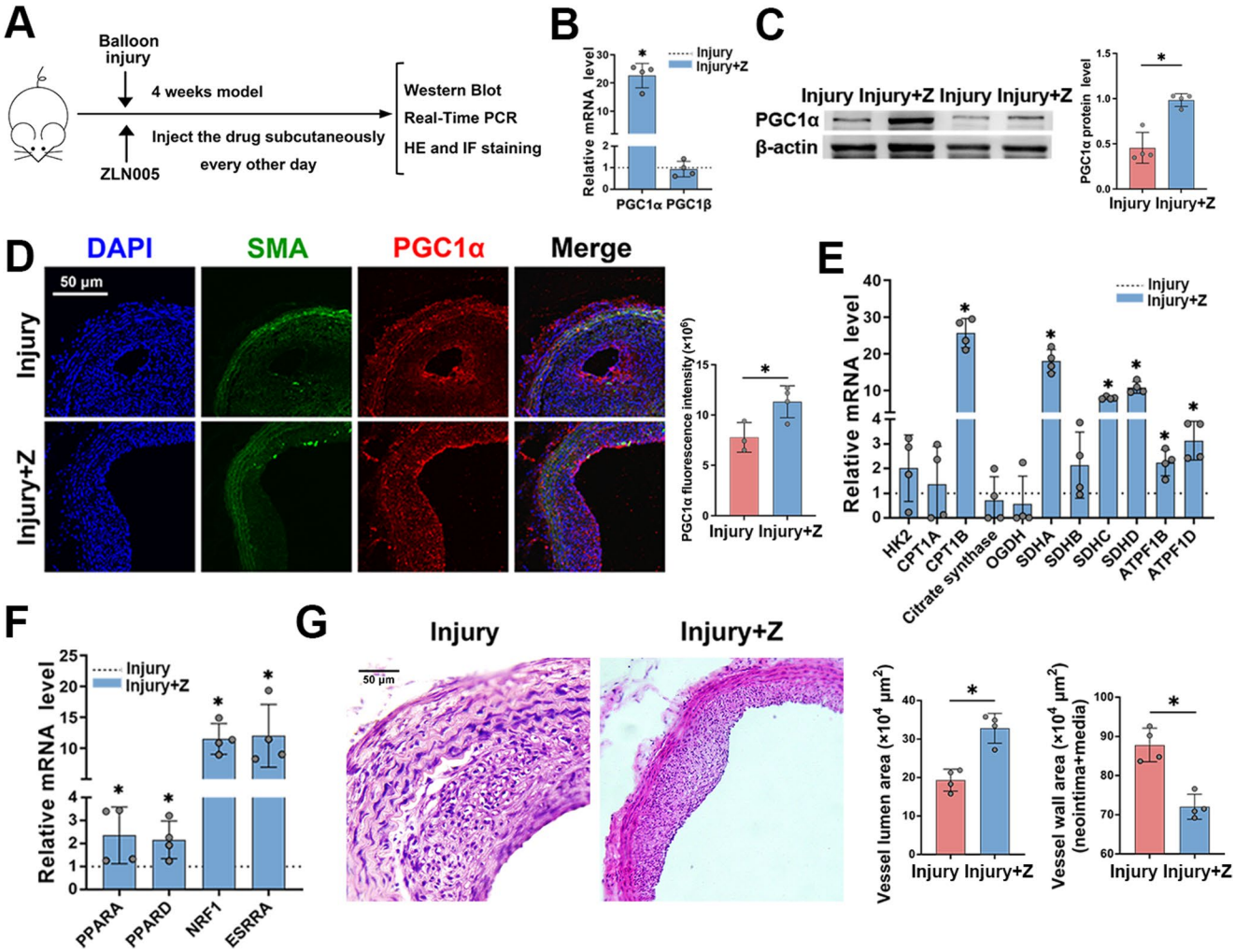

Fig. 8 The PGC1α activator ZLN005 effectively improved mitochondrial function and inhibited VSMC hyperproliferation in vivo. (A) Flow chart of the treatment with ZLN005 in the intimal injury model and the experiments after 4 weeks. (B) The mRNA levels of PGC1α and PGC1β in the carotid artery in the injured group compared with those in the treatment group were determined by qRT–PCR ($n=4$). (C) The protein level of PGC1α in the carotid artery in the injured group with or without ZLN005 treatment was determined by western blotting. (D) Representative immunofluorescence images of the carotid artery in the injured group and ZLN005 treatment group at 4 weeks ($n\geq3$). Blue: DAPI; green: SMA; red: PGC1α. Scale bar = 50 μm. (E) The mRNA levels of rate-limiting enzymes in the carotid artery in the injured group compared with those in the treatment group were determined by qRT–PCR ($n=4$). (F) The mRNA levels of target genes of PGC1α in the carotid artery in the injured group compared with those in the treatment group were determined by qRT–PCR ($n=4$). (G) Representative HE-stained images of carotid arteries from the injured group and treatment group at 4 weeks ($n=4$). Scale bar = 50 μm. *P* values were calculated by a two-tailed Mann–Whitney test. The values are the means ± *SD*. * $P<0.05$

upstream molecules, and Smad3 was selected by IPA. Smad3 is a transcription factor that is active when it is phosphorylated. In response to TGF-β stimulation [43], p-Smad2 and p-Smad3 form a complex with Smad4 that is translocated into the nucleus to regulate downstream gene expression [44–46]. Smad3-deficient mice exhibit increased neointimal hyperplasia and reduced matrix deposition in response to vascular injury in atherosclerotic vascular diseases [47, 48], suggesting that Smad3 may regulate the function of VSMCs to limit the extent of neointimal hyperplasia. In heart failure, the transcription-mediated protein RMP activates the TGF-β/Smad3 signaling pathway, promotes PGC1α expression, maintains PGC1α-dependent mitochondrial biogenesis function, and protects cardiomyocytes from injury [49]. We observed that cyclic stretch did not significantly alter TGFβ1 protein level in VSMCs or TGFβ1 secretion levels in the culture medium (Supplemental Figs. 6A and B). However, inhibition of TGFβ using a neutralizing antibody markedly reduced the phosphorylation level of Smad3 (Supplemental Figs. 6C and D), suggesting that Smad3 activation was most likely regulated by TGFβ. In our study, p-Smad3 was demonstrated to be activated to upregulate the expression of PGC1α upon cyclic stretch at 6 h. The expression of PGC1α was also decreased by the Smad3-specific phosphorylation

inhibitor SIS3. These results suggest that Smad3 may affect mitochondrial function in VSMCs by regulating the expression of PGC1α.

Moreover, our results demonstrated that most mitochondrial components exhibited a downregulation at the transcriptional level following intimal injury, whereas all four SDH subunits (SDHA, SDHB, SDHC, and SDHD) demonstrated significant upregulation. Notably, these four SDH subunits are exclusively encoded by nuclear genes, in contrast to other oxidative phosphorylation complexes whose subunits are encoded by both mitochondrial and nuclear genomes [50]. Therefore, we propose that the sustained nuclear transcription of SDH genes may represent a key mechanism underlying the observed elevation in SDH subunit levels.

Furthermore, we incorporated a widely recognized PGC1α agonist, ZLN005, into our study. It is based on the extensive use of ZLN005 in numerous studies, which has consistently demonstrated its efficacy and reliability in activating PGC1α. For instance, Wu et al. demonstrated that ZLN005 enhances the expression of PGC1α and its target gene, increases muscle ATP levels, and reduces ROS [51]. Moreover, Shipra et al. found that targeted ZLN005 delivery or cardiomyocyte-specific PGC1α overexpression significantly improves cardiomyopathy treatment [52].

Regarding the mechanism of ZLN005-induced activation of PGC1α, Zhang et al. proposed that ZLN005 might activate AMPK by increasing the ADP/ATP ratio, ultimately regulating PGC1α expression [41]. However, changes in the ADP/ATP ratio may exert their effects not only through AMPK activation but also via multiple pathways that influence cellular metabolism and other signaling cascades. Therefore, ZLN005 may exhibit pleiotropic effects, and further study is needed to explore the underlying mechanism of its effect on PGC1α. Such investigations are crucial for substantiating our findings and advancing our understanding of its broader biological implications.

In conclusion, the results of the present study suggest that PGC1α activated by p-Smad3 may inhibit the abnormal proliferation of VSMCs through regulating mitochondrial function and that physiological cyclic stretch plays a vital role in this process. In the case of intimal injury, the increased expression of PGC1α can partially restore the functional activity of mitochondria, thus alleviating the excessive proliferation of VSMCs (Fig. 9). Our data suggest a possible novel mechanism by which Smad3 and PGC1α regulate mitochondrial function and VSMC abnormal proliferation during neointimal hyperplasia. This study may provide feasible and underlying therapeutic treatments for the abnormal proliferation of VSMCs after intimal injury and potential targets for treating mitochondrial dysfunction.

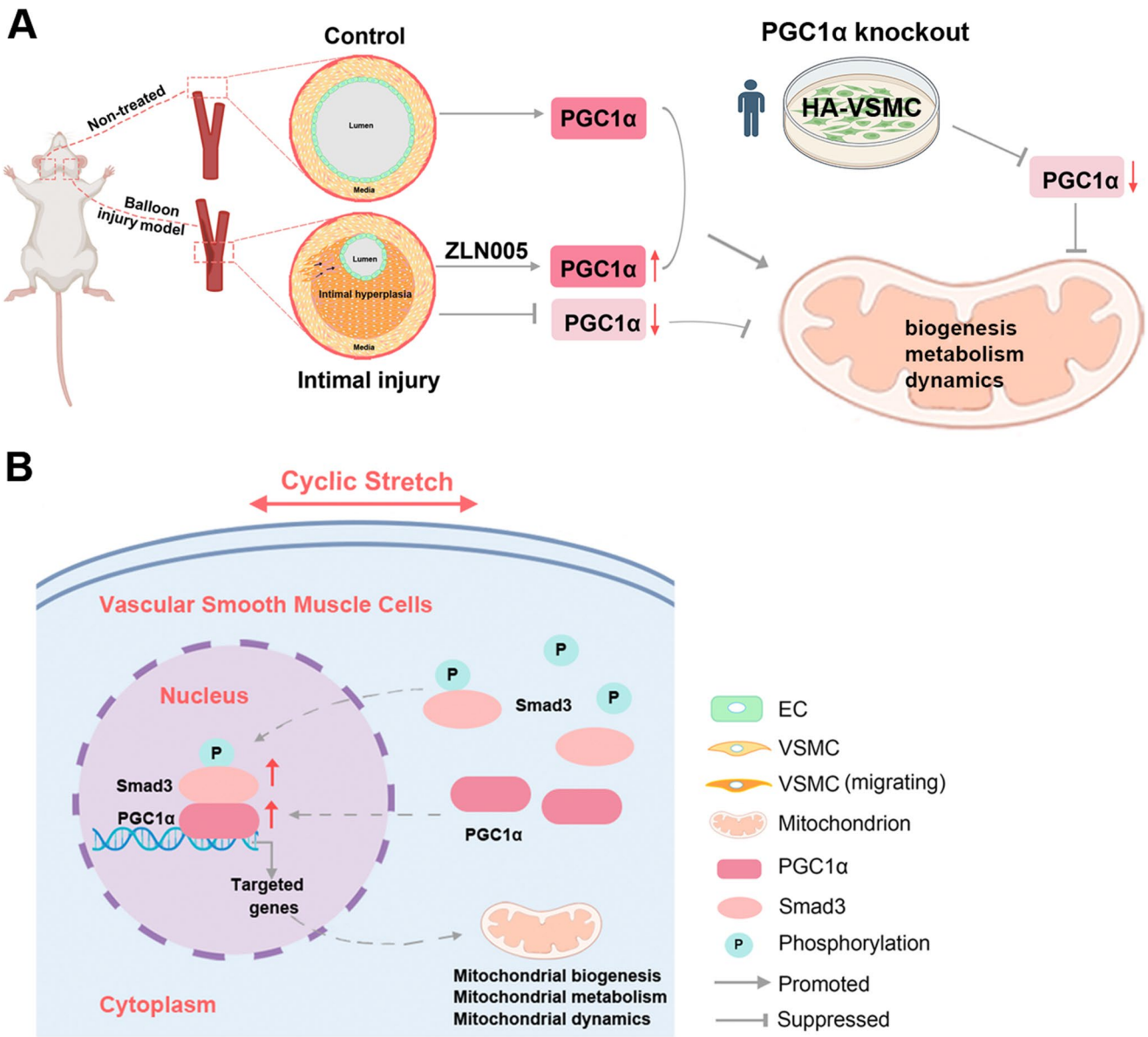

Fig. 9 Schematic diagram of PGC1α regulation of VSMC mitochondrial function in vivo and in vitro. (A) In vivo, the intimal injury arteries were harvested after four weeks, and the opposite carotid artery without treatment was collected for the control. Intimal injury caused neointimal hyperplasia and decreased the expression of PGC1α, which consequently suppressed mitochondrial biogenesis, metabolism, and dynamics. However, the subcutaneous injection of ZLN005 every other day reversed these effects and partially restored mitochondrial function. In addition, an abnormal ultrastructure of mitochondria occurred in human plaques, and PGC1α knockout in human aortic VSMCs impaired mitochondrial metabolism. (B) In vitro, cyclic stretch activated Smad3 phosphorylation and then increased the expression levels of PGC1α in VSMCs. PGC1α further activated the transcription of downstream target genes involved in mitochondrial biogenesis, metabolism, and dynamics, ultimately promoting the mitochondrial function of VSMCs

Supplementary Information The online version contains supplementary material available at https://doi.org/10.1007/s00018-025-05790-x.

Acknowledgements This study was supported by grants from the Natural Science Foundation of Shanghai (25ZR1401176), the National Key Research and Development Program of China (2021YFA1000200 and 2021YFA1000203), the Clinical Research Program of Shanghai Ninth People's Hospital, Shanghai Jiao Tong University School of Medicine (YBKB202224), and the National Natural Science Foundation of China (No.12072197).

Author contributions S.Z. and Y.H. designed research; S.Z., J.Y., H.B., Z.L., M.Z. and W.T., performed research; K.Y., X.Z.,Y.Q. and YL.H. provided intellectual input and materials, M.Z., S.Z., T.T. analyzed data; S.Z., M.Z., and Y.H. wrote the paper.

Data Availability The datasets used and/or analyzed during the current study are available from the corresponding author on reasonable request.

Declarations

The authors declare that they have no conflict of interest regarding the publication of this article.

References

1. Doenst T, Haverich A, Serruys P et al (2019) PCI and CABG for treating stable coronary artery disease: JACC review topic of the week. J Am Coll Cardiol 73:964–976
2. Wu B, Mottola G, Schaller M et al (2017) Resolution of vascular injury: specialized lipid mediators and their evolving therapeutic implications. Mol Aspects Med 58:72–82
3. Yu E, Mercer J, Bennett M (2012) Mitochondria in vascular disease. Cardiovasc Res 95:173–182
4. Jannig PR, Dumesic PA, Spiegelman BM, Ruas JL (2022) SnapShot: regulation and biology of PGC-1α. Cell 185:1444–1444e1
5. Handschin C, Spiegelman BM (2006) Peroxisome proliferator-activated receptor gamma coactivator 1 coactivators, energy homeostasis, and metabolism. Endocr Rev 27:728–735
6. Lehman JJ, Barger PM, Kovacs A et al (2000) Peroxisome proliferator-activated receptor gamma coactivator-1 promotes cardiac mitochondrial biogenesis. J Clin Invest 106:847–856
7. Agudelo LZ, Ferreira DMS, Dadvar S et al (2019) Skeletal muscle PGC-1alpha1 reroutes kynurenine metabolism to increase energy efficiency and fatigue-resistance. Nat Commun 10:2767
8. Forte M, Schirone L, Ameri P et al (2021) The role of mitochondrial dynamics in cardiovascular diseases. Br J Pharmacol 178:2060–2076
9. Tian L, Cao W, Yue R et al (2019) Pretreatment with Tilianin improves mitochondrial energy metabolism and oxidative stress in rats with myocardial ischemia/reperfusion injury via AMPK/SIRT1/PGC-1 alpha signaling pathway. J Pharmacol Sci 139:352–360
10. Niu X, Pu S, Ling C et al (2020) LncRNA Oip5-as1 attenuates myocardial ischaemia/reperfusion injury by sponging miR-29a to activate the SIRT1/AMPK/PGC1alpha pathway. Cell Prolif 53:e12818
11. Wang WB, Li HP, Yan J et al (2019) CTGF regulates Cyclic stretch-induced vascular smooth muscle cell proliferation via microRNA-19b-3p. Exp Cell Res 376:77–85
12. Bao H, Li ZT, Xu LH et al (2021) Platelet-derived extracellular vesicles increase Col8a1 secretion and vascular stiffness in intimal injury. Front Cell Dev Biol 9:641763
13. Trapnell C, Roberts A, Goff L et al (2012) Differential gene and transcript expression analysis of RNA-seq experiments with tophat and cufflinks. Nat Protoc 7:562–578
14. Huang da W, Sherman BT, Lempicki RA (2009) Systematic and integrative analysis of large gene lists using DAVID bioinformatics resources. Nat Protoc 4:44–57
15. Raudvere U, Kolberg L, Kuzmin I et al (2019) G:Profiler: a web server for functional enrichment analysis and conversions of gene lists (2019 update). Nucleic Acids Res 47:W191–W198
16. Gillespie M, Jassal B, Stephan R et al (2022) The reactome pathway knowledgebase 2022. Nucleic Acids Res 50:D687–D692
17. Dai L, Li C, Shedden KA, Misek DE et al (2009) Comparative proteomic study of two closely related ovarian endometrioid adenocarcinoma cell lines using cIEF fractionation and pathway analysis. Electrophoresis 30:1119–1131
18. Wu M, Zhang C, Xie M et al (2021) Compartmentally scavenging hepatic oxidants through AMPK/SIRT3-PGC1α axis improves mitochondrial biogenesis and glucose catabolism. Free Radic Biol Med 168:117–128
19. Huang Q, Su H, Qi B et al (2021) A SIRT1 activator, ginsenoside rc, promotes energy metabolism in cardiomyocytes and neurons. J Am Chem Soc 143:1416–1427
20. Toutouzas K, Colombo A, Stefanadis C (2004) Inflammation and restenosis after percutaneous coronary interventions. Eur Heart J 25:1679–1687
21. Tian R, Colucci WS, Arany Z et al (2019) Unlocking the secrets of mitochondria in the cardiovascular system: path to a cure in heart failure-a report from the 2018 National heart, lung, and blood Institute workshop. Circulation 140:1205–1216
22. Chiu JJ, Chien S (2011) Effects of disturbed flow on vascular endothelium: pathophysiological basis and clinical perspectives. Physiol Rev 91:327–387
23. Qi YX, Yao QP, Huang K et al (2016) Nuclear envelope proteins modulate proliferation of vascular smooth muscle cells during Cyclic stretch application. Proc Natl Acad Sci U S A 113:5293–5298
24. Yan J, Wang WB, Fan YJ et al (2020) Cyclic stretch induces vascular smooth muscle cells to secrete connective tissue growth factor and promote endothelial progenitor cell differentiation and angiogenesis. Front Cell Dev Biol 8:606989
25. Kim HK, Kang YG, Jeong SH et al (2018) Cyclic stretch increases mitochondrial biogenesis in a cardiac cell line. Biochem Biophys Res Commun 505:768–774
26. Vasquez-Trincado C, Garcia-Carvajal I, Pennanen C et al (2016) Mitochondrial dynamics, mitophagy and cardiovascular disease. J Physiol 594:509–525
27. Marsboom G, Toth PT, Ryan JJ et al (2012) Dynamin-related protein 1-mediated mitochondrial mitotic fission permits hyperproliferation of vascular smooth muscle cells and offers a novel therapeutic target in pulmonary hypertension. Circ Res 110:1484–1497
28. Huynh DTN, Heo KS (2021) Role of mitochondrial dynamics and mitophagy of vascular smooth muscle cell proliferation and migration in progression of atherosclerosis. Arch Pharm Res 44:1051–1061
29. Deng Y, Li S, Chen Z et al (2021) Mdivi-1, a mitochondrial fission inhibitor, reduces angiotensin-II- induced hypertension by mediating VSMC phenotypic switch. Biomed Pharmacother 140:111689
30. Nguyen EK, Koval OM, Noble P et al (2018) CaMKII (Ca^{2+}/calmodulin-dependent kinase II) in mitochondria of smooth muscle cells controls mitochondrial mobility, migration, and Neointima formation. Arterioscler Thromb Vasc Biol 38:1333–1345
31. Abhijit S, Bhaskaran R, Narayanasamy A et al (2013) Hyperinsulinemia-induced vascular smooth muscle cell (VSMC) migration and proliferation is mediated by converging mechanisms of mitochondrial dysfunction and oxidative stress. Mol Cell Biochem 373:95–105

32. Badran A, Nasser SA, Mesmar J et al (2020) Reactive oxygen species: modulators of phenotypic switch of vascular smooth muscle cells. Int J Mol Sci 21(22):8764
33. Puigserver P, Wu Z, Park CW et al (1998) A cold-inducible coactivator of nuclear receptors linked to adaptive thermogenesis. Cell 92:829–839
34. Liang H, Ward WF (2006) PGC-1alpha: a key regulator of energy metabolism. Adv Physiol Educ 30:145–151
35. Tiraby C, Langin D (2005) [PGC-1alpha, a transcriptional coactivator involved in metabolism]. Med Sci (Paris) 21:49–54
36. Finck BN, Kelly DP (2006) PGC-1 coactivators: inducible regulators of energy metabolism in health and disease. J Clin Invest 116:615–622
37. van der Pluijm I, Burger J, van Heijningen PM et al (2018) Decreased mitochondrial respiration in aneurysmal aortas of Fibulin-4 mutant mice is linked to PGC1A regulation. Cardiovasc Res 114:1776–1793
38. Wen JJ, Cummins CB, Szczesny B et al (2020) Cardiac dysfunction after burn injury: role of the AMPK-SIRT1-PGC1alpha-NFE2L2-ARE pathway. J Am Coll Surg 230:562–571
39. Yang XY, Li QJ, Zhang WC et al (2020) AMPK-SIRT1-PGC1alpha signal pathway influences the cognitive function of aged rats in sevoflurane-induced anesthesia. J Mol Neurosci 70:2058–2067
40. Kant S, Tran KV, Kvandova M et al (2022) PGC1alpha regulates the endothelial response to fluid shear stress via telomerase reverse transcriptase control of Heme oxygenase-1. Arterioscler Thromb Vasc Biol 42:19–34
41. Zhang LN, Zhou HY, Fu YY et al (2013) Novel small-molecule PGC-1α transcriptional regulator with beneficial effects on diabetic db/db mice. Diabetes 62:1297–1307
42. Zhao M, Li Y, Lu C et al (2023) PGC1α degradation suppresses mitochondrial biogenesis to confer radiation resistance in glioma. Cancer Res 83:1094–1110
43. Liu X, Sun Y, Constantinescu SN et al (1997) Transforming growth factor beta-induced phosphorylation of Smad3 is required for growth Inhibition and transcriptional induction in epithelial cells. Proc Natl Acad Sci U S A 94:10669–10674
44. Souchelnytskyi S, Tamaki K, Engstrom U et al (1997) Phosphorylation of Ser465 and Ser467 in the C terminus of Smad2 mediates interaction with Smad4 and is required for transforming growth factor-beta signaling. J Biol Chem 272:28107–28115
45. Heldin CH, Miyazono K, ten Dijke P (1997) TGF-beta signalling from cell membrane to nucleus through SMAD proteins. Nature 390:465–471
46. Derynck R, Zhang Y, Feng XH (1998) Smads: transcriptional activators of TGF-beta responses. Cell 95:737–740
47. Yokote K, Kobayashi K, Saito Y (2006) The role of Smad3-dependent TGF-beta signal in vascular response to injury. Trends Cardiovasc Med 16:240–245
48. Kobayashi K, Yokote K, Fujimoto M et al (2005) Targeted disruption of TGF-beta-Smad3 signaling leads to enhanced neointimal hyperplasia with diminished matrix deposition in response to vascular injury. Circ Res 96:904–912
49. Zhang J, Sheng J, Dong L et al (2019) Cardiomyocyte-specific loss of RNA polymerase II subunit 5-mediating protein causes myocardial dysfunction and heart failure. Cardiovasc Res 115:1617–1628
50. Hock DH, Robinson DRL, Stroud DA (2020) Blackout in the powerhouse: clinical phenotypes associated with defects in the assembly of OXPHOS complexes and the mitoribosome. Biochem J 477(21):4085–4132
51. Wu H, Lu C, Li X et al (2022) Insufficient sleep disrupts glucose metabolism during pregnancy by inhibiting PGC-1α. Ann Transl Med 10(22):1241
52. Shipra, Tembhre MK, Hote MP et al (2023) PGC-1α agonist rescues doxorubicin-induced cardiomyopathy by mitigating the oxidative stress and necroptosis. Antioxid (Basel) 12(9):1720